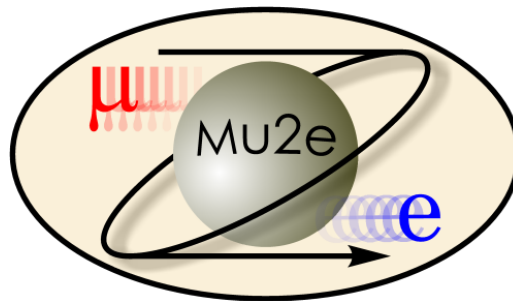# Antiproton background of the Mu2e experiment and the vertical misalignment of the Mu2e beamline

Intern : Nigrelli Giulia
Supervisor: Pavel Murat

Contents

1 Introduction

Mu2e experiment will search for the neutrinoless $\mu^- \to e^-$ conversion in the field of an aluminum nucleus.

The total expected background in Mu2e Run I is 0.11 ± 0.03 events, and the antiproton background, $0.01 \pm 0.003(stat) \pm 0.010(syst)$, is about 10% of the total [1].

The report discusses the antiproton background of the Mu2e experiment. As it will be explained, the antiproton background is sensitive to the vertical misalignment of the Mu2e beamline. Therefore, it is important to measure the misalignment in situ. The report introduces a data-driven technique of measuring the beamline misalignment.

The material is organized as follows. Section 2 describes the Mu2e experiment. Section 3 presents the antiproton background. Section 4 explains the alignment in the apparatus. Section 5 presents the vertical misalignment and a method to measure it from the data. Section 6 presents the initial simulations made and the discussion of the results.

2 Mu2e experiment

2.1 Mu2e apparatus

The Mu2e experiment primary proton beam with $E_{kin} = 8.9\,GeV$ is extracted from the Fermilab Delivery Ring. The three superconducting solenoids, in order: **production solenoid** (PS), **transport solenoid** (TS) and **detector solenoid** (DS) lead particles from the production target, in the PS, to the stopping target, in the DS. The inner part of all three solenoids is kept at vacuum. Figure 1 presents a schematic view of the Mu2e apparatus.

The beam is impinging on a ~ 1.6 interaction lenghts-long tungsten **production target** (PT) located in the middle of the PS. The beam has a pulsed time structure, with $250\,ns$ wide pulses separated by $1695\,ns$.
The PS graded magnetic field reaches its maximal strength of 4.6 T downstream of the PT.

Muons forming the Mu2e muon beam are produced in $\pi^- \to \mu^- \bar{\nu}_\mu$ decays of charged pions. Muons produced backwards as well as muons produced in the forward direction and reflected in the PS magnetic mirror are captured by the S-shaped transport solenoid and travel through it towards the DS. Muons are produced in both PS and TS.

The TS magnetic field is also graded, from $\sim 2.5\,T$ at the entrance to $\sim 2.1\,T$ at the end. Three collimators placed inside the TS, *COL1* at the entrance, *COL3* in the middle and *COL5* at the exit, define the TS momentum acceptance, limiting it to momenta below $\sim 100\,MeV/c$.

The TS shape rotates the direction of the magnetic field, and while moving through the TS the charged particles of different signs drift vertically in opposite directions. In the middle of the TS, the positive and negative particles are well separated in the vertical direction, and the offset vertically opening of the COL3 collimator selects the beam sign. A rotation of the COL3 allows to switch the beam sign from negative to positive and vice versa - see Figure 6.

The DS magnetic field is graded in the upstream part, $B = 2\,T \to 1\,T$, and uniform, $B \sim 1\,T$, in the downstream region. The **stopping target** (ST) is made of 37 aluminum annular foils spaced $2.2\,cm$ apart. Each foils is $105\,\mu m$ thick. The ST is placed in the graded magnetic field region of the DS on the DS axis. The particle detectors, the tracker and the calorimeter, are located in the downstream part of the DS.
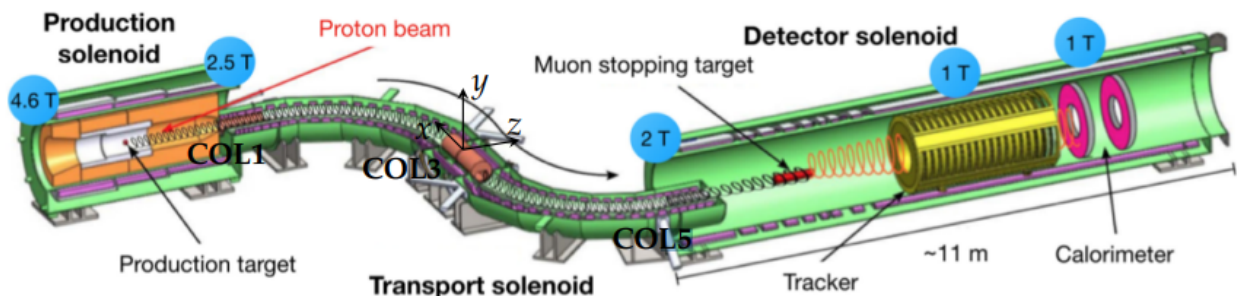

Figure 1: Schematic view of the Mu2e apparatus. The center of the Mu2e reference frame is located in the COL3 collimator center, its y-axis points upwards, the z-axis is parallel to the DS axis and points downstream, and the x-axis completes the right-handed reference frame.

A fraction of muons, 1/3 of the total that reaches the ST, stops and interacts with the Al atomic field. These muons have $p < 50\,MeV/c$. The *stopped muon rate*, that is the number of stopped muons for primary proton, is $N_{POT}^{\mu^-} = 1.6 \times 10^{-3}$ from the muon beam simulations.

Muons stopped in the target rapidly decay to a orbital 1s in the ^{27}Al atoms, where they could undergo the process $\mu^- \to e^-$. Being a two body decay, the electron momentum distribution is expected to be monochromatic. In addition, the nucleus in the final state remains in the ground state therefore the conversion electron has an energy equal to:

$$E_{CE} = m_\mu - E_{recoil} - E_{bind} = 104.97\,MeV; \tag{1}$$

where m_μ is the muon mass, E_{recoil} is the recoil energy of the target nucleus, and E_{bind} is the binding energy of the 1s state of the muonic atom.

2.2 Backgrounds

Several background processes can generate electrons with energy $\sim 105\,MeV$.

- **Cosmic rays**, mostly muons, interact in the detector sensitive volume and produce electrons with $p \sim 100\,MeV/c$. The Cosmic Ray Veto system (CRV) suppresses this background by four orders of magnitude.

- Muons captured by Al atoms **decay in orbit (DIO)** producing electrons with a momentum spectrum extending up to $105\,MeV/c$. Suppression of this background requires a detector with an high momentum resolution $\Delta p < 1\,MeV/c$.

- **Antiprotons** annihilate in the stopping target produce $p \sim 100\,MeV/c$ electrons. Antiproton flux is suppressed with several absorption element placed inside the TS.

- **Radiative capture of pions** (RPC) stopping in the ST produce $p \sim 105\,MeV/c$ electrons. Suppressing this background requires delayed measurements compared to the arrival of the proton pulse at the PT by hundred nanoseconds.

- **Radiative muon capture** (RMC), analogous to RPC. The kinematic endpoint, $E \sim 102\,MeV$, is lower than RPC.

- **Electrons** with $p \sim 100\,MeV$ scattering in the Al target, a delayed measure is needed to suppress this background.

- **Decays in flight** of μ^- and π^- producing $p \sim 100\,MeV$ electrons in the DS which are detected by the tracker.

The physics processes listed above have different time dependencies. For $\mu^- \to e^-$ conversion, DIO and RMC the time dependence is defined by the lifetime of a muonic Al atom, $864 \pm 1\,ns$. Cosmic rays background is distributed uniformly in time. RPC timing depends on the pion lifetime. Beam electrons and decays in flight are negligible and related to not extinct protons timing.

2.3 Mu2e detector

The detector structure includes a straw tracker to measure momenta of the secondary charged particles, an electromagnetic calorimeter to estimate the energy and the Cosmic Ray Veto system (CRV).

The tracker consists of 18 tracking stations. In total there are 20736 straws tubes of $5\,mm$ diameter each, filled with a $80\% : 20\%\,Ar : CO_2$ mixture at a pressure of $1\,atm$.

The hit coordinate along the straw is reconstructed using the difference between two timing measurements obtained by reading out each straw from both ends. For $100\,MeV$ electrons, the momentum resolution of the tracker is $\Delta p_{trk} < 300\,KeV/c$FWHM. For muons with the same momentum, the resolution is worse, by a factor $1.5 \div 2$, due to the higher energy losses.

The calorimeter is composed by two annular disks, with an internal radius of $37\,cm$ and an external radius of $66\,cm$, positioned at $70\,cm$ distance from each other. Each disk is assembled from 674 undoped CsI crystals, $3.3 \times 3.4 \times 20cm^3$ in size. Crystals are read out by two silicon photomultipliers (SiPMs).

The tracker is placed about $3\,m$ downstream of the stopping target in the uniform magnetic field region of the DS. The calorimeter is located immediately downstream of the tracker. The two detectors together provide efficient particle identification.

The data read out from the detectors are digitized and transmitted through optical fibers by the data acquisition system (DAQ).

2.4 Analysis and simulation software

We simulate production of particles in the production target and trace the beam up to the stopping target. The particles produced in the stopping target are simulated taking into account the detector geometry. The simulation framework provides reconstruction algorithm and visualization tools.

Once the events are reconstructed, the reconstructed tracks are parameterized with the following parameters:
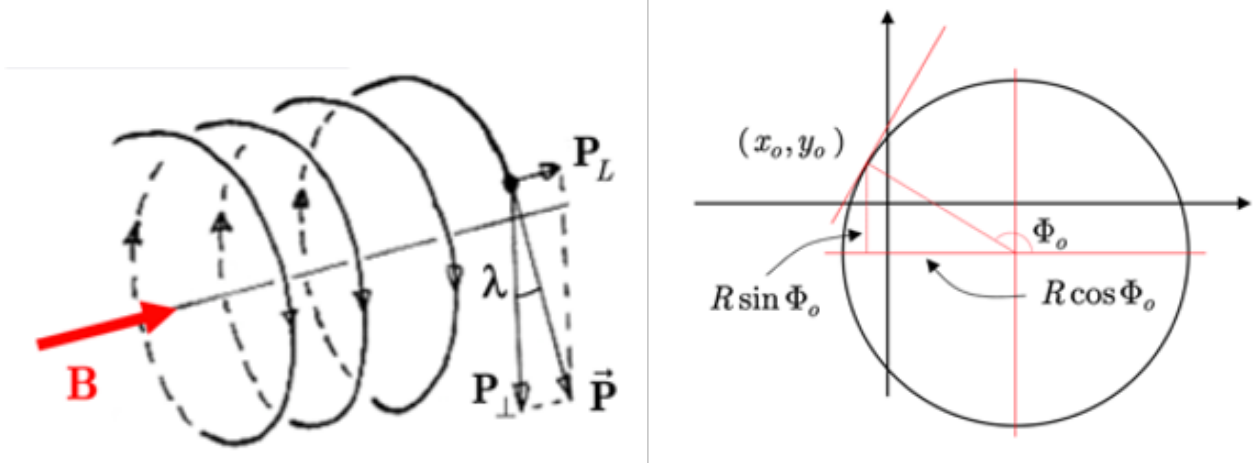
$$P : (d_0, \phi_0, \omega, z_0, tan\lambda); \tag{2}$$

Figure 2: Left: Helix trajectory. Right: xy-view of the track.

where d_0 is the distance of the point of closest approach from the solenoid system axis and the sign depends on the momentum direction in that point; ϕ_0 is the momentum direction in the point of closest approach; $\omega = 1/R$; z_0 is the z-coordinate of the point of closest approach; $90° - \lambda$ is the petch angle between p and xy plane.

The experimental signature of a $\mu^- \rightarrow e^-$ conversion is a peak around $105\ MeV/c$ in the momentum distribution. The *estimated total background* in the Mu2e Run 1 is 0.105 ± 0.032, but the experimental rate is unknown. An estimate of small backgrounds is an experimentally challenging task.
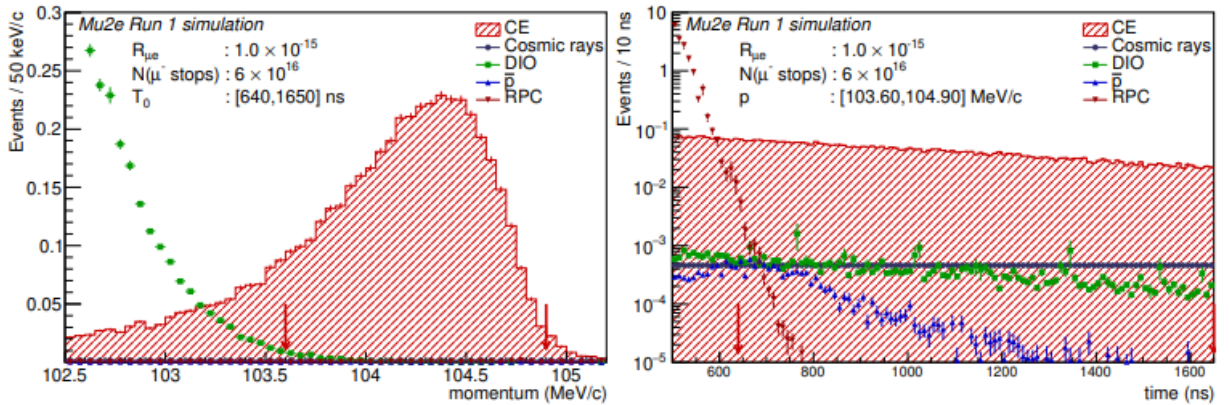

Figure 3: Left: Peak around $105\ MeV/c$ in the electron momentum distribution in red, with backgrounds. Right: Zoom on the backgrounds. It is visible that for the assumed value of $R_{\mu e}$ the estimated total background is lower than the peak.

3 Antiproton background

Antiproton background is due to the annihilation of antiprotons in the stopping target. The antiprotons are produced in the interaction of the proton beam in the tungsten target. Such antiprotons can pass through the TS and reach the stopping target in the DS. The annihilation in the stopping target could result in a signal-like conversion electron.

The delayed measurement window can't sufficiently suppress this background. To suppress this background, several thin absorbers are placed at the entrance and at the center of the TS. The antiproton background is sensitive to the vertical misalignment of the collimator.

One of the biggest uncertainty on the estimate of the antiproton background comes from the angular dependence of the antiproton production cross section. Currently available data on the antiproton production at beam momentum around $10\,GeV$ cover the range between $0° - 120°$ as seen in figure 5.
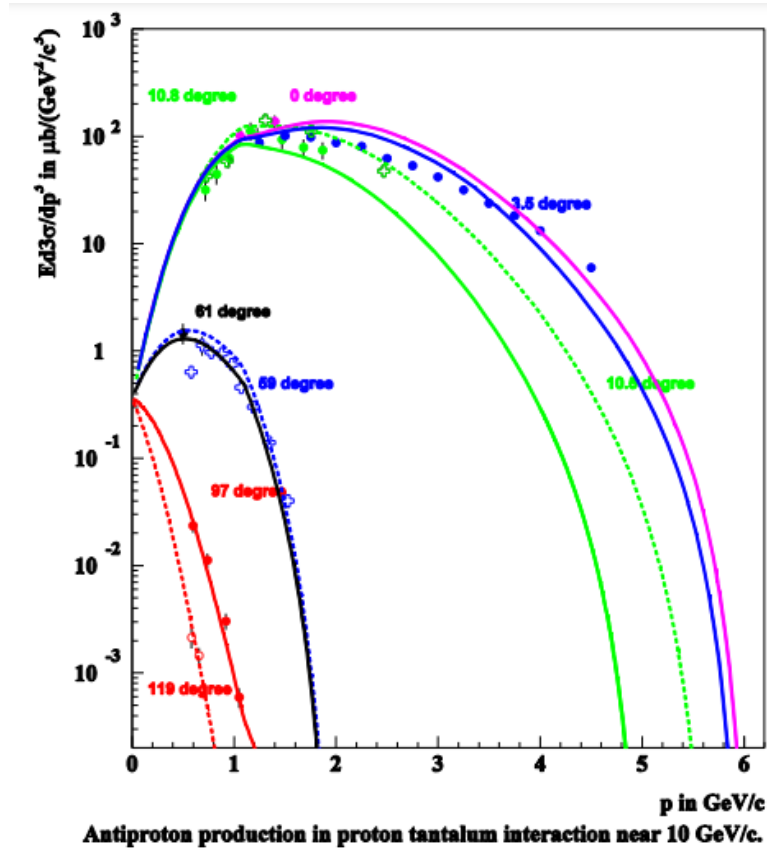

Figure 4: Angular dependence of the antiproton production cross section in p-Ta interactions at $10\,GeV/c$.

Relevant for Mu2e experiment are antiproton productions around $180°$. Moreover, the available data are at energy around $\sim 10\,GeV/c$ while the Mu2e proton beam has a momentum of $8.9\,GeV/c$, the cross section changes by a factor about 2 from $10\,GeV/c$ to $8.9\,GeV/c$.

The *antiproton background* estimate is $(8.1 \pm 0.7(stat) \pm 8.1(syst)) \times 10^{-3}$, the systematic relative error is assumed to be 100%.

4 Apparatus alignment

Mu2e beams are unique, one of positively charged particles and one of negatively charged particles. The beams are helical and move through the TS.

The S-shape solenoid consist in two C-shape section, as shown in figure 5. The B-field, directed toward the TS axis, rotates implying the vertical drift of particles. This results in a vertical separation that reaches its maximum in the middle of the TS. This feature makes it easy to select the negatively charged beam.
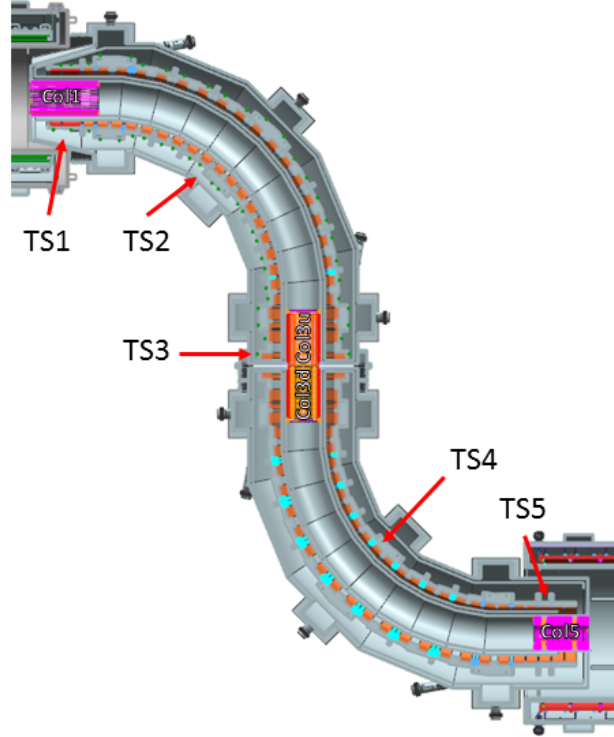

Figure 5: Schematic xz-view of the transport solenoid. At COL3 the magnetic field is directed along x axis, while at COL5 it is oriented towards z axis.

The particles move along a curved magnetic field line, hence they experience a centrifugal force due to the field curvature. Therefore, they drift perpendicular to both the centrifugal force and B.

Stating the radius of curvature of the magnetic field lines R_c, then:

$$\mathbf{F}_{curv} = \frac{mv_\parallel^2}{R_c^2}\mathbf{R}_c; \tag{3}$$

and so

$$\mathbf{v}_{curv} = \frac{E}{0.3q}\frac{\mathbf{R}_c \times \mathbf{B}}{R_c^2\,B^2}\beta_\parallel^2 \tag{4}$$

The drift is proportional to the momentum and its direction depends on the particle charge. As a consequence, negatively charged particles drift upwards due to the first curvature of the B-field, from TS1 to TS3, then they drift downwards from TS3 to TS5. The behaviour of positively charged particles is opposite.

Because of the vertical drift, the alignment of elements in the TS becomes relevant since it could significantly modify the space of possible stopped trajectory.

In particular, Col3 is the key element in the system alignment because it selects the beam charge but also partially suppresses the antiproton background. The Col3 consists in two parts Col3u and Col3d. These collimators select the charge of the beam through the opening position (figure 6), that is placed at the top in the default configuration in order to have a μ^- beam.
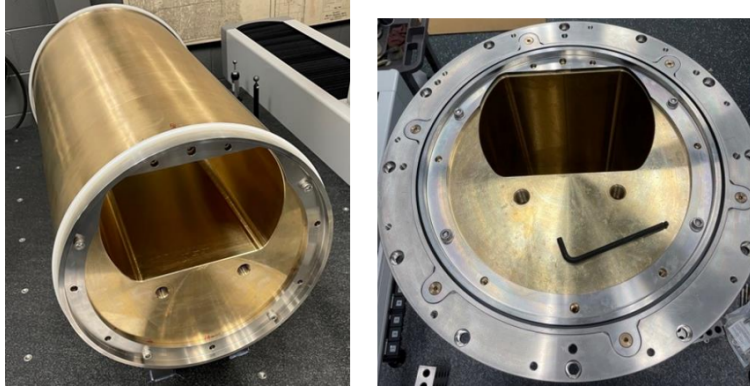
Figure 6: Pictures of the COL3 placed in the middle of the TS3.

A titanium window placed between the two parts of Col3 stops antiprotons with $p < 100 \, MeV$. A wedge shape absorber located immediately after the window improves the antiproton rejection.

Figure 7 and 8 schematically show the trajectories of positively and negatively particles as they travel through the TS:

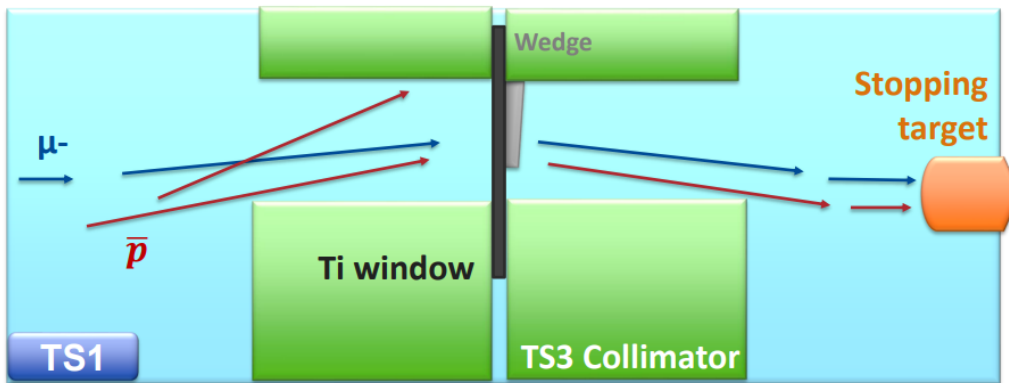- **Negatively charged particles**

Figure 7: Trajectories of negatively charged particles inside the TS3.

The presence of the absorbers reduces the intensity of the muon beam of a few percent.

Most antiprotons are absorbed in the TS1, the remaining part hits the walls of the collimators due to the drift. The fraction of antiprotons with $p > 100 \, MeV/c$ manages to enter the Col3u and, if it is not absorbed by the titanium window or by the wedge, it begins to drift downwards coming out of the Col3d. In this way they exit the TS and reach the stopping target where they annihilate.
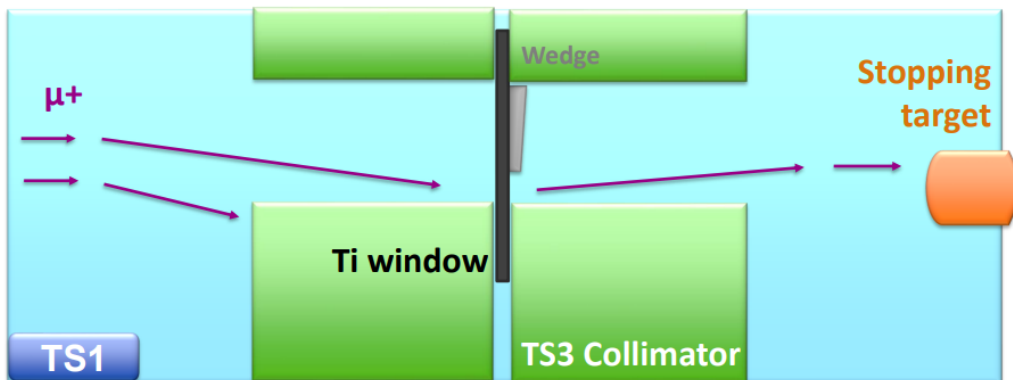
- **Positively charged particles**

Figure 8: Trajectories of positively charged particles inside the TS3.

Most μ^+s are stopped by col3u due to the downward drift. However, a fraction of the order of 10^{-3} passes through and reaches the stopping target.

Coordinate distributions of μ^+ and μ^- reaching the stopping target are expected to be different. In particular, for μ^- the distribution should be symmetric with respect to zero instead for the μ^+ it should be shifted upwards. We expect to see all the μ^+ concentrated in the upper part of the stopping target. These differences should lead to same differences in the distribution of muon stopping point. These distributions will be shown and commented in the Section 6.

5 Vertical misalignment

The antiproton background may be sensitive to the relative misalignment between the production target, Col3 and the stopping target along the y-direction.

Indeed, if the Col3 is in an upper position compared to the default one then more antiprotons can pass through the collimators. Vice versa, if the Col3 is lower then less antiprotons can reach the stopping target, reducing the background.

The vertical misalignment also affects the μ^+. The presence of the misalignment would change the ratio of the stopping rates μ^+/μ^-.

Therefore the misalignment could be measured from the ratio of the stopping rates μ^+/μ^-. In addition, as the coordinate distribution of μ^+ is asymmetric that should results in an asymmetry in the angular distributions of the reconstructed positrons.

We expect to have all of the reconstructed tracks for positrons in the upper part of the tracker, as shown in figure 9.
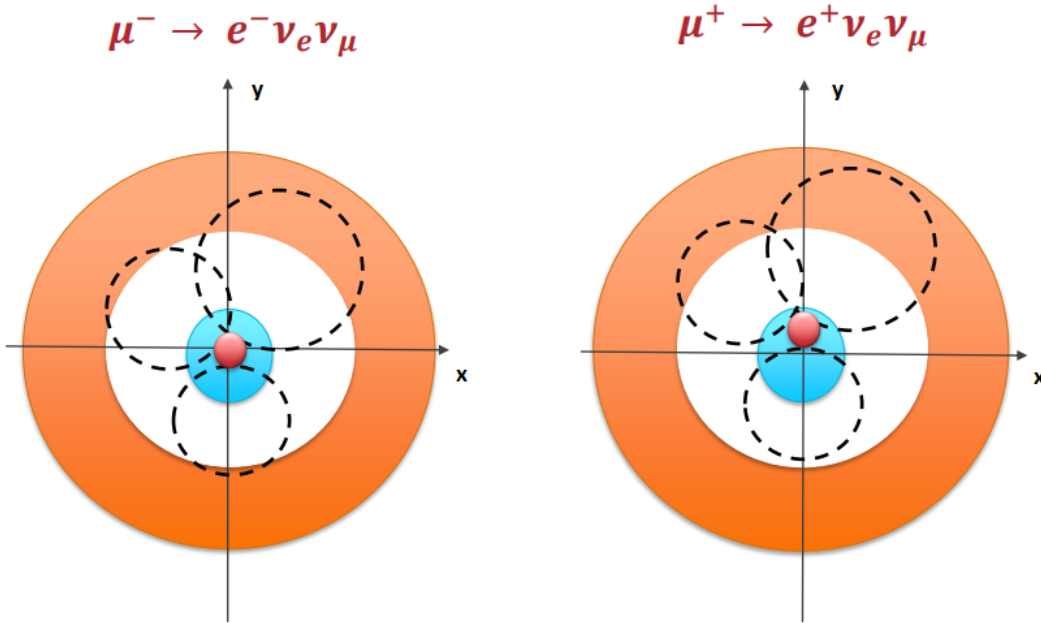

Figure 9: Reconstructed track distributions for Michell decay of μ^+ and μ^-. In orange the xy section of the tracker, in red the xy view of the stopping target and in red the xy view of the beam spot. The dashed line are the recontructed tracks of electrons (left) and positrons (right).

We define:

$$tg(\phi) = \frac{p_y}{p_x}; \tag{5}$$

Where p is the momentum vector of the reconstructed track in the point of closest approach.

The radius of the helix track is:

$$R = \frac{p_\perp (GeV)}{B(T)\,q\,0.3} \implies d = R + d_0 \implies X_c = d \times cos(\phi) \quad Y_c = d \times sin(\phi); \tag{6}$$

where d_0 has been defined in Section 2; d is the distance between the axis origin and the center; (X_c, Y_c) are the centre coordinates.
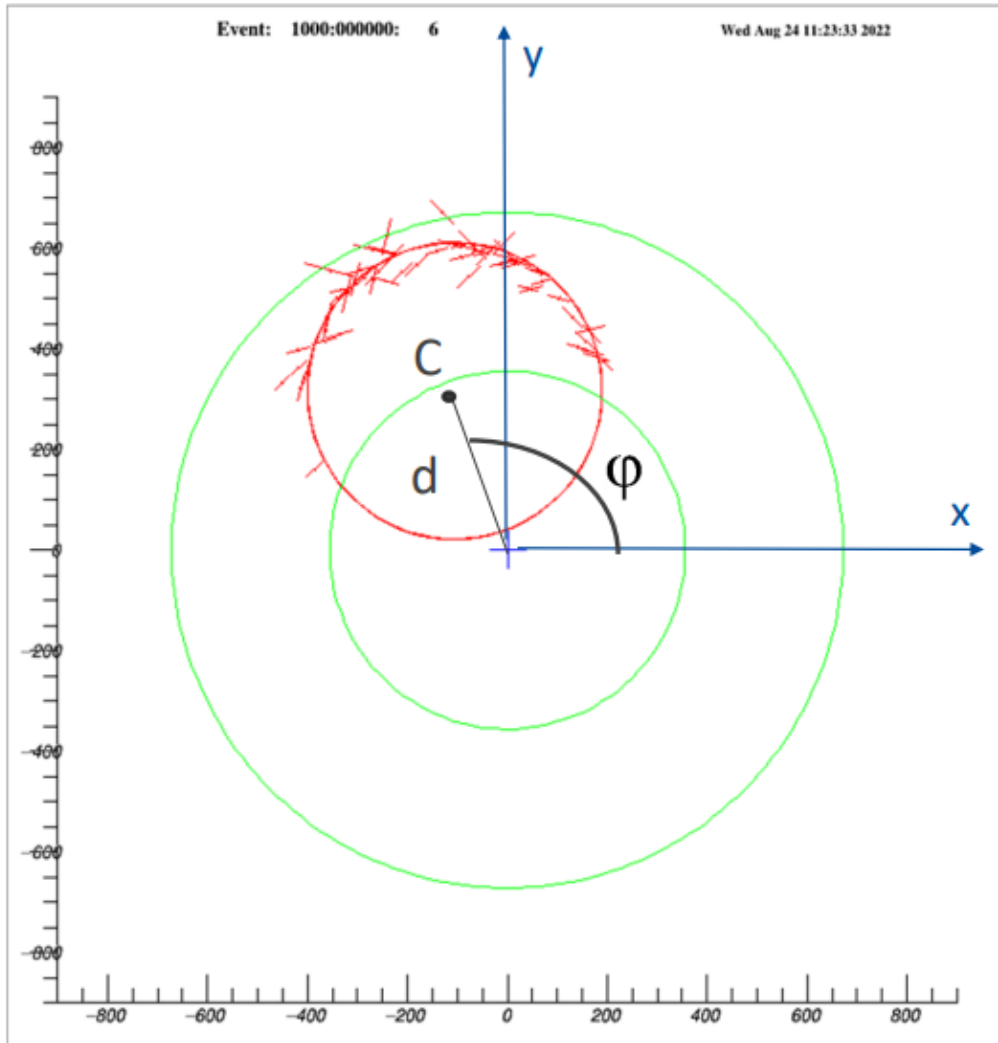
Figure 10: Event display of a reconstructed conversion electron track. In green the xy section of the tracker. The red circle is the Monte Carlo simulated track and the red segments are the straw hits of the particle.

An asymmetry in the vertical distributions of μ^+ stops should lead to a wave-shaped ϕ distribution of the reconstructed positron tracks. The vertical misalignment can be estimated by the amplitude.

6 Results and comments

We use the Mu2e simulation framework to estimate the sensitivity of the asymmetry to the vertical misalignment.

10^8 proton interactions in the production target have been simulated. The Monte Carlo simulation predicts the ratio of the stopping rates equal to $\mu^+/\mu^- = 2 \times 10^{-3}$.

The total number of μ^+ which stopped in the stopping target was ~ 600, to simulate higher statistics of $\mu^+ \to e\nu_\mu\nu_e$ decays each stop μ^+ has been reused 200 times. The number of stopped μ^- was 500 times larger than μ^+ hence resamplig was not required. The magnetic field in the detector solenoid to reconstruct the $p \sim 50\,MeV/c$ positrons and electrons has been reduced to $B = 0.5\,T$.

The following figures show the distributions of interaction vertex coordinates for μ^+ and μ^-.

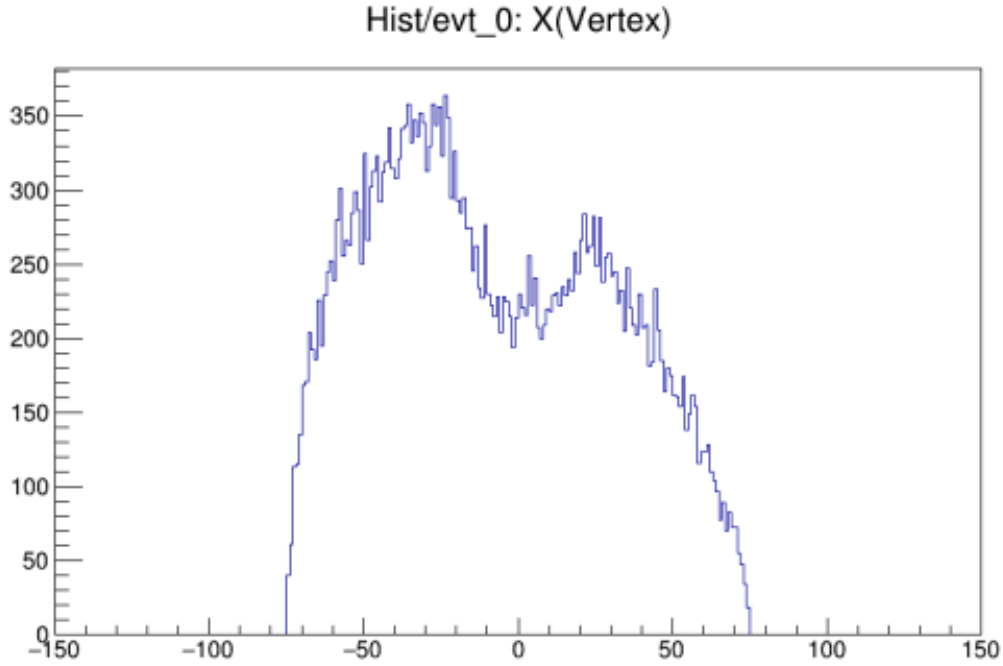
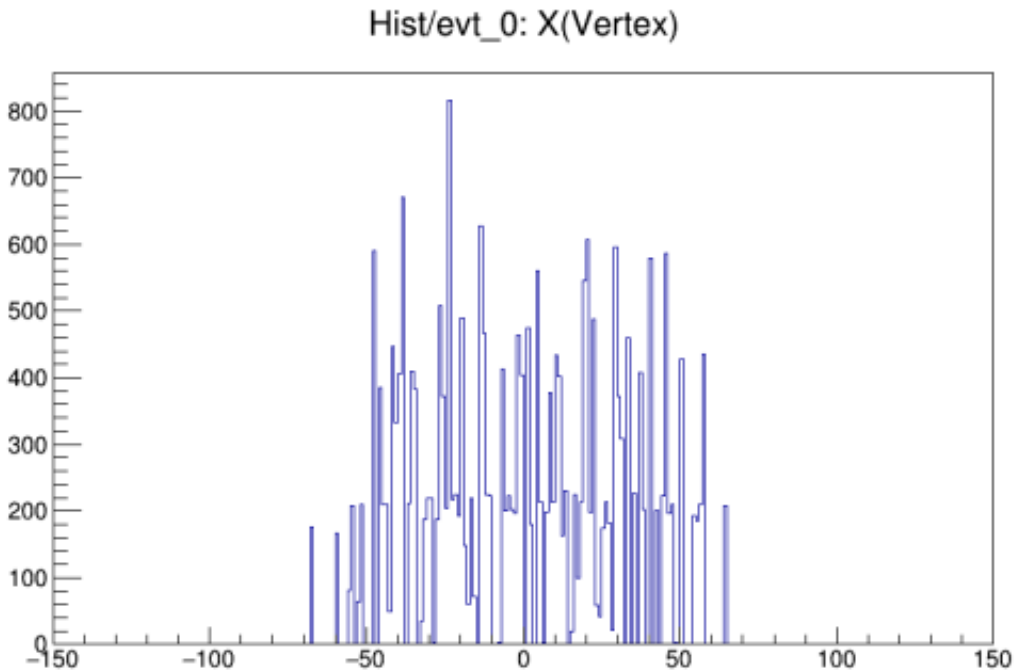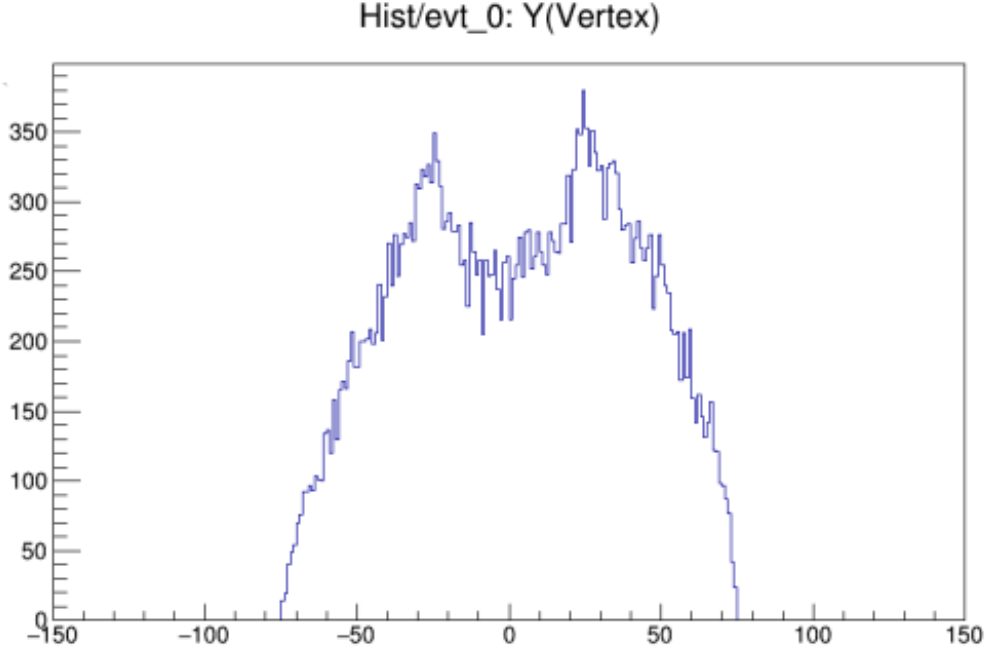Figure 11: Distribution of x-coordinate of interaction vertices for μ^-.

Figure 12: Distribution of x-coordinate of interaction vertices for μ^+.

The distribution of x-coordinate of interaction vertices for μ^- presents an unexpected asymmetry. The distribution of μ^+ also appears asymmetric. The large statistical fluctuations in figure 12, due to oversampling, make it difficult to derive a conclusion.

A structure around x=0, visible in figure 11, is due to an opening $r \sim 2\,cm$ in the center of the stopping target.

Figure 13: Distribution of y-coordinate of interaction vertices for μ^-.

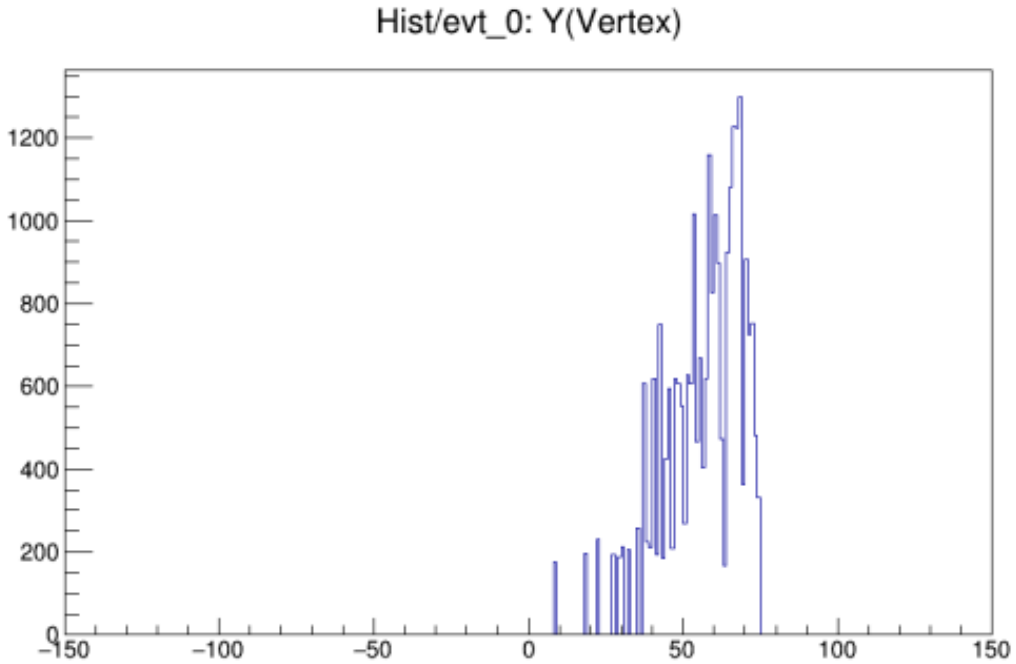
Figure 14: Distribution of y-coordinate of interaction vertices for μ^+.

As expected, the distribution of y-coordinate of μ^+ stops (figure 14) shows an asymmetry, all μ^+ stops are concentrated in the upper part of the stopping target.

For μ^-, the y-distribution is more symmetric than the x-distribution, but it is still possible to observe a small asymmetry (more particle in the upper part of the ST).

The asymmetries of the μ^+ and μ^- distributions are not observable. The reconstructed parameters for $e^\pm$ tracks should be reflect the same asymmetries.

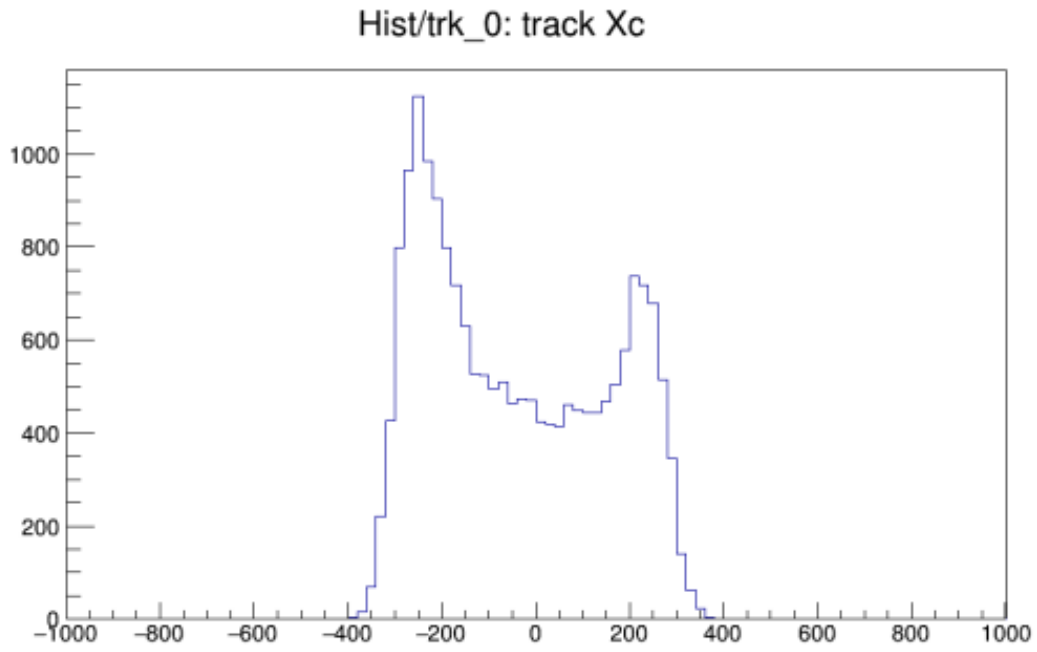Figure 15 and 16 show the distributions of the coordinate centre of the reconstructed tracks for $e^\pm(6)$.

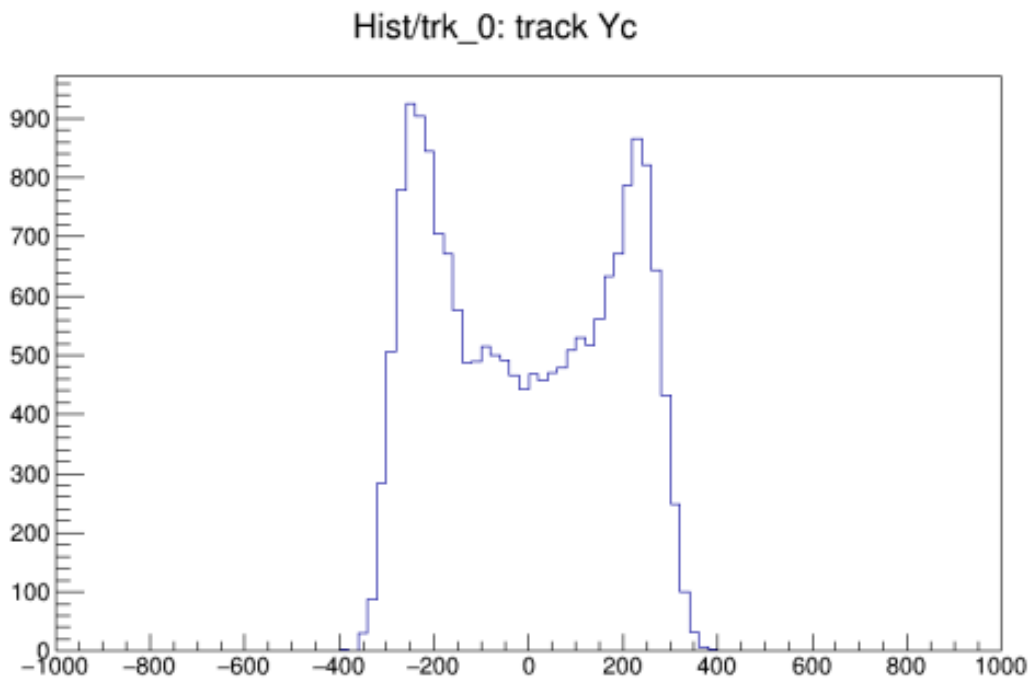Figure 15: Distribution of x_c, x-coordinate of reconstructed track centre for e^-.

Figure 16: Distribution of y_c, y-coordinate of reconstructed track centre for e^-.

Asymmetry of the distribution in figure 11 is reflected in the distribution of electron xc. The origin of this asymmetry is under investigation.

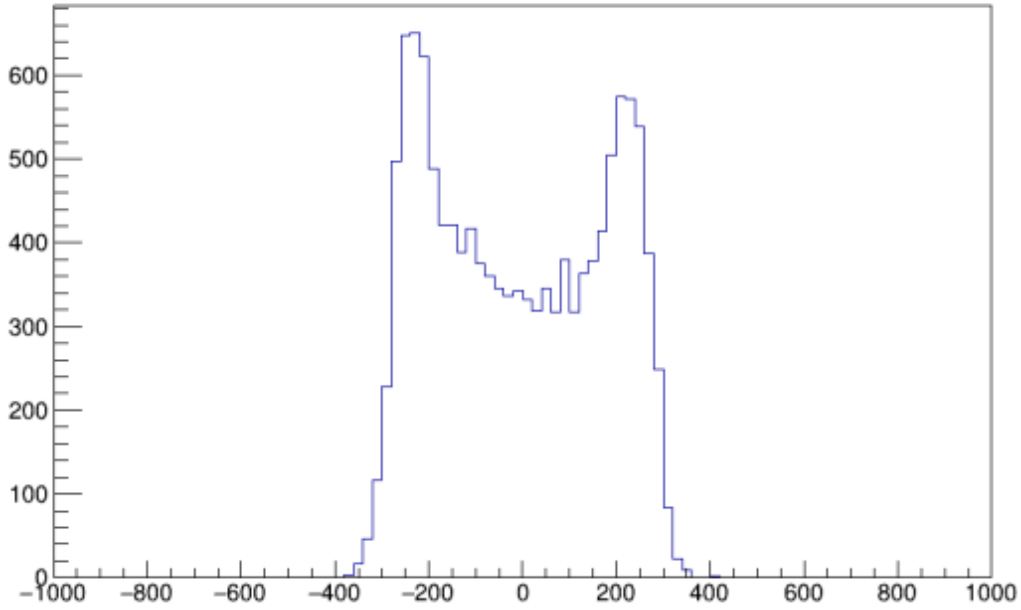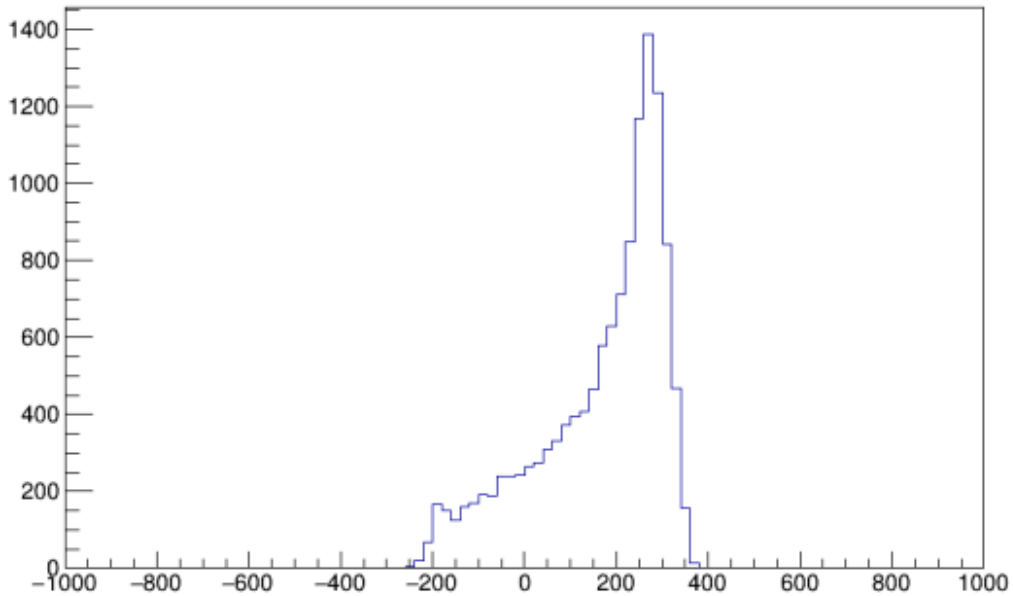Figure 17: Distribution of x_c, x-coordinate of reconstructed track centre for e^+.

Figure 18: Distribution of y_c, y-coordinate of reconstructed track centre for e^+.

The x-distribution for positrons is more symmetric than the electrons one. The y-distribution shows that the most part of the positrons trajectories are contained in the upper half of the detector.

Figure 17 and 18 show that the parameters of the reconstructed trajectories are sensitive to the initial asymmetry of the production vertices and therefore to the misalignment of the beamline.

The beamline misalignment should affect the asymmetry of the distributions of μ^+ stops and through that asymmetry of the distributions of the reconstructed track parameters.

Even better way to study the asymmetry is to study the angular distributions. Figure 19 shows the distribution of the reconstructed ϕ angle, introduced in Section 5, for electron tracks.
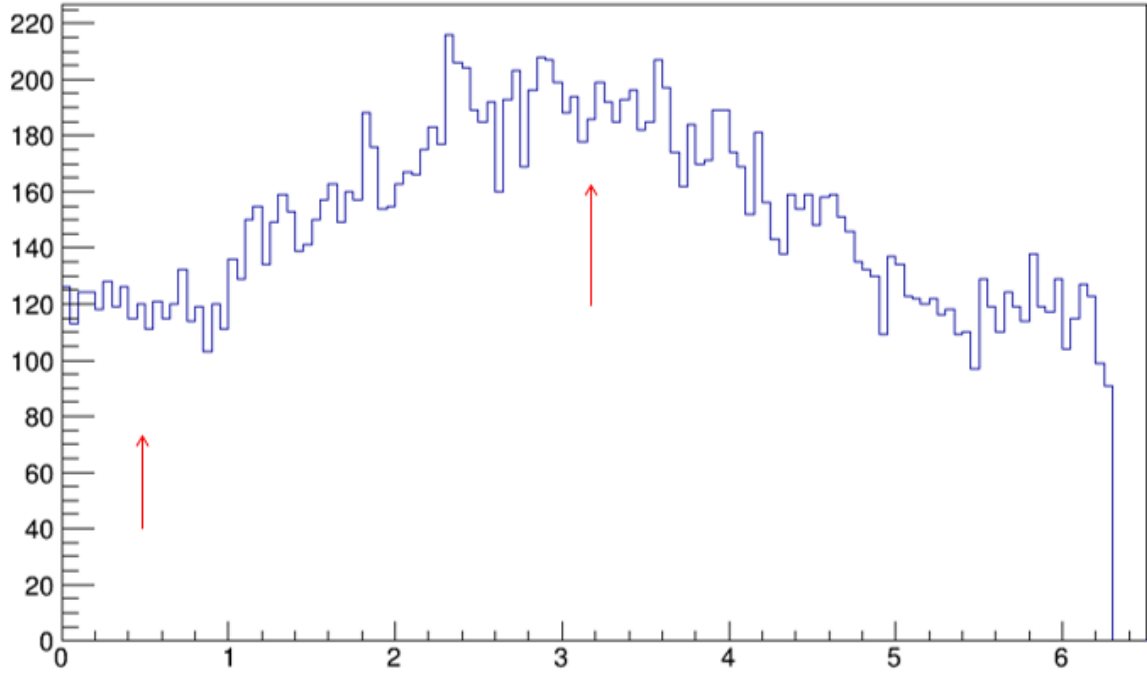
Figure 19: ϕ distribution for e^-.

Instead of the flat distribution, figure 19 shows a wave with a maximum around π which has the same origin as the offset x_c distribution for electrons in figure 15.
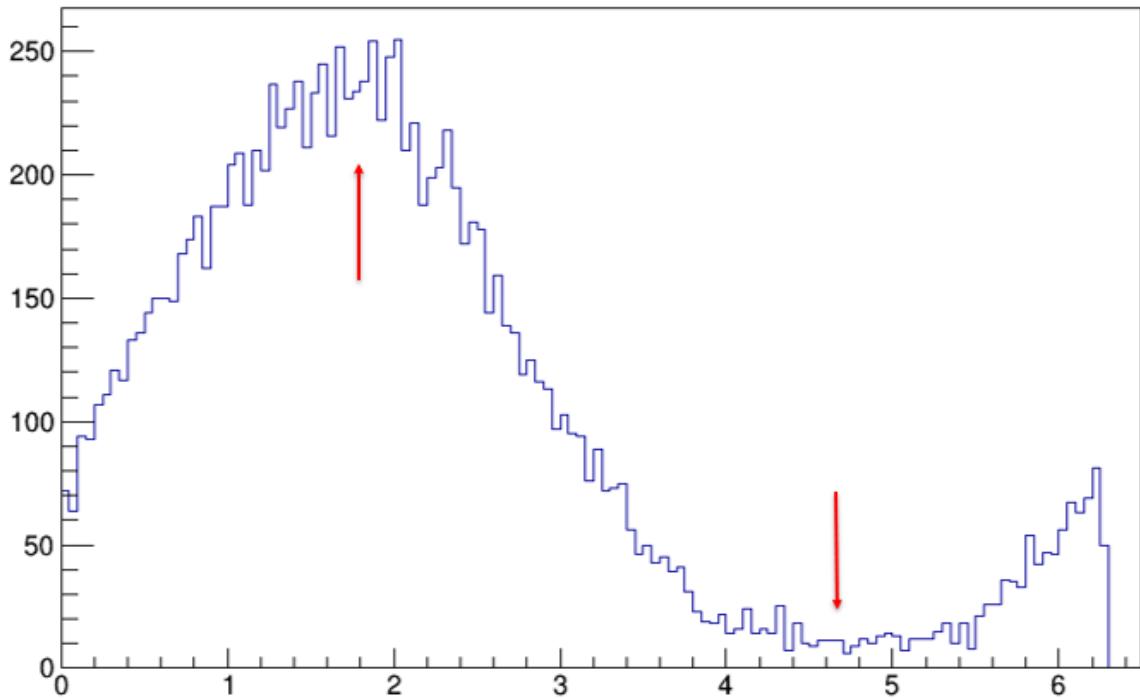

Figure 20: ϕ distribution for e^+.

Shown in figure 20 the ϕ distribution for the positrons shows a wave with a maximum around $\pi/2$ corresponding to a vertical offset distribution for the positron production vertices (figure 18).

Note, that the maximum and the minimum of the distribution are not exactly at $\pi/2$ and $3\pi/2$ due to the x_c-asymmetry shown in figure 17. The difference between the maximum and the minimum is a measure of the asymmetry and therefore is sensitive to the vertical misalignment.

14

7 Conclusions

In conclusion, we have shown that the asymmetries in the reconstructed parameters of electrons and positrons tracks from $\mu \to e\nu\nu$ decays are sensitive to the effects of the beamline misalignment. These asymmetries could be used to study the vertical misalignment of the beamline, which is needed for the antiproton background estimates.

An initial study has found an unexpected asymmetry of the x_c distribution of the μ^- stops. This asymmetry could be caused to the reduced magnetic field, which is presently under investigation.

References

[1] Mu2e Collaboration. *Mu2e Run I Sensitivity Projections for the Neutrinoless $\mu^- \to e^-$ Conversion Search in Aluminum*. 2022. DOI: https://doi.org/10.48550/arxiv.2210.11380. URL: https://arxiv.org/abs/2210.11380.